The Journal of Engineering

The 7th International Conference on Renewable Power Generation (RPG 2018)

IET Journals
The Institution of Engineering and Technology

New control paradigm for both islanded and grid-connected operation of PMSG-based wind turbine

eISSN 2051-3305
Received on 6th November 2018
Accepted on 10th January 2019
doi: 10.1049/joe.2018.9359
www.ietdl.org

Muftau O. Baruwa[1] ✉, *Meghdad Fazeli*[1], *Augustine M. Egwebe*[1]

[1]*Swansea University, UK*

✉ *E-mail: 750340@swansea.ac.uk*

Abstract: This article proposes a new control paradigm for the seamless operation of a permanent magnet synchronous generator (PMSG) based wind energy conversion system (WECS) in both islanded and grid-connected modes. Conventionally, grid-connected WECS are controlled to extract the maximum power from the wind, known as maximum power point tracking (MPPT). However, in islanded operation, the objective is to control the power generated from the WECS to match the load demand, which here is called load following power generation (LFPG). This article proposes a power management system (PMS) which integrates the MPPT and LFPG capabilities of the WECS into a single-control paradigm. This enables the WECS to seamlessly achieve MPPT in grid operation, LFPG in islanded mode and low-voltage ride-through (LVRT) during fault. The proposed scheme is validated using MATLAB/SIMULINK simulations.

1 Introduction

The increasing energy demands, depletion of fossil fuel reserves, and global warming have accelerated the implementation of renewable energy sources (RESs)-based distributed generators (DGs). DG units are usually connected in a cluster to form a microgrid which can operate independently or in parallel with the grid network [1, 2].

DG units designed for islanded operation are usually termed as grid-forming units; this is because they are equipped with control structures which enable regulation of the local voltage and frequency within stipulated standards. In this mode of operation, the power generated by the DG must match the load demand to maintain stable operating conditions [3, 4].

When DG units are operating in grid-connected mode, a synchronism mechanism, usually a phase-locked loop (PLL), is implemented to keep the DG units synchronised with the grid. This units are primarily required to exchange active and reactive power with the grid, since voltage and frequency are maintained by the grid [1, 5]. However, in the event of a fault on the grid side, the microgrid must be disconnected after a stipulated time frame. This will lead to power interruption to the local loads if the DG units are not equipped with grid-forming ability. Hence, to maximise the available RES and enhance power reliability to local loads, DG units must be capable of operating seamlessly in both grid-connected and islanded mode [3].

Several literatures have discussed control techniques of WECS in grid-connected or islanded mode; however, only a handful of previous arts have discussed control of the WECS in both modes. Erlich *et al.* [6] proposed a direct voltage control technique which regulates the voltage of the WECS following a fault on the grid side. An emergency-frequency controller was also designed to reduce power generation when frequency rises above nominal value. However, this control was only tested for transient periods of fault condition and its capability to effectively support local loads was not evaluated. In [7], the authors implemented the conventional droop control in both grid-connected and islanded operating modes. However, there is no provision for MPPT during normal operation. In addition, the adopted grid synchronisation scheme will not work for multiple systems, as this will lead to conflicting phase angles between the output from the droop and the grid voltage. Rizo *et al.* [8] proposed a single control structure for grid and islanded mode. The authors suggested using pitch control and breaking chopper to dump the excess power in islanded mode. However, the passive islanding technique implemented for transition from grid-connected to islanded mode suffers from a relatively large non-detection zone (NDZ) [9].

As discussed above, most of the earlier works do not guarantee optimal operating conditions in both operating modes simultaneously. In addition, they required some switching mechanism (from grid-connected to islanded mode of operation and vice versa), which may undermine the seamless operation of the system. This paper proposes a single-control paradigm for permanent magnet synchronous generator (PMSG)-based WECS that enables (1) seamless transition from grid-connected to islanded operation (and vice versa); (2) maximum power point tracking (MPPT) and load following power generation (LFPG) in grid-connected and islanded modes, respectively, (3) low-voltage ride-through (LVRT) capability during faults.

This paper is organised as follows: A comprehensive description of the proposed control structure is presented in Section 2. Simulation results have been presented in Section 3 to corroborate the proposed control technique. Section 4 concludes the paper.

2 Proposed method

For the sake of simplicity in the presentation of the results, the understudy system (Fig. 1) consists of only one PMSG WECS. However, the control method can be implemented for large wind farms as well as DFIG-based WECS.

2.1 Wind turbine modelling

The mechanical power P_m captured by the wind turbine is expressed by the following equation [10]:

$$P_m = 0.5\rho \mathrm{A} \mathrm{v}^3 C_p(\lambda, \beta) \tag{1}$$

$$T_m = \frac{P_m}{\omega_r} \tag{2}$$

where ρ is the air density in Kg/m^3, A is the area swept by the turbine blades in m^2, υ is the wind speed in m/s, T_m is mechanical torque in Nm, ω_r is the rotor speed in rad/s and C_p (λ, β) is the power coefficient. The C_p (λ, β) is a non-linear function of the tip speed ratio λ and the pitch angle β, which is given by (3) and (4) [10]:

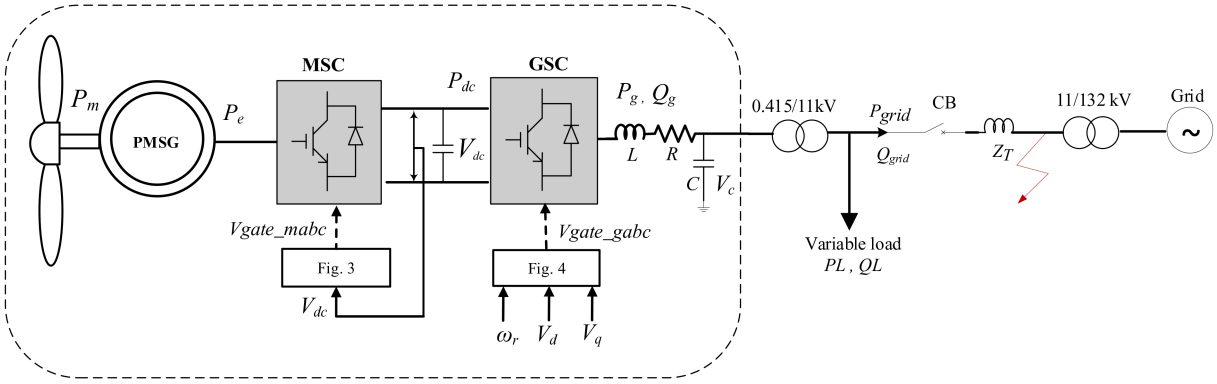

Fig. 1 *Configuration of the system understudy*

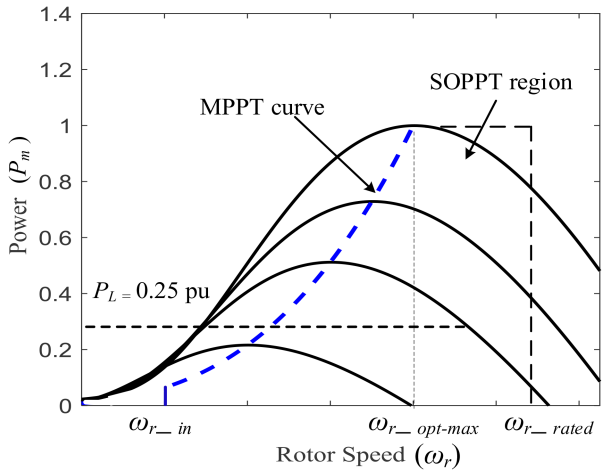

Fig. 2 *Power–speed characteristics of wind turbine*

$$C_p(\lambda,\beta)=0.5176\left(\frac{116}{\lambda_i}-0.4\beta-5\right)e^{-21/\lambda_i}+0.0068\lambda_i \tag{3}$$

$$\frac{1}{\lambda_i}=\frac{1}{\lambda+0.08\beta}-\frac{0.035}{\beta^3+1} \tag{4}$$

Fig. 2 illustrates the power-speed characteristics of the wind turbine, where ω_{r_in} refers to the minimum rotor speed at which the WECS begins to operate, $\omega_{r\_opt\text{-}max}$ ($=\omega_{r\text{-}base}=1$ pu) is the maximum operating speed of the rotor on the MPPT curve and ω_{r_rated} is the rated speed of the rotor. When WECS are connected to the grid, they are usually operated at MPPT. The MPPT curve defines the optimal rotor speed ($\omega_r=\omega_{r\_opt}$) that the WECS must maintain to extract the maximum power from the wind ($P_m=P_{max}$, where P_{max} is the maximum power available from the wind).

However, for islanded operation, the mechanical power generated P_m must be curtailed to match the load demand P_L ($P_m=P_L$, $P_m\leq P_{max}$). To achieve this, the WECS is required to operate in the suboptimal power point region (SOPPT) which is to the right of the MPPT curve (see Fig. 2), which guarantees stable operation and stores excess energy as kinetic energy (KE) [7, 10, 11]. As illustrated in Fig. 2, for operation in SOPPT $\omega_r>\omega_{r\_opt}$ when $P_L<P_{max}$. In this scheme, the standard pitch angle control [12] is only required when the rotor speed exceeds its rated value $\omega_r>\omega_{r\_rated}$, or the mechanical power exceeds its rated capacity $P_m>P_{max}$.

The drive train of the WECS is governed by (5) [13]:

$$J\frac{d\omega_r}{dt}=T_m-T_e-B\omega_r \tag{5}$$

where J is the equivalent inertia of the turbine and the generator in Kgm^2, B is the friction coefficient in Nms, and T_e is the electrical torque in Nm.

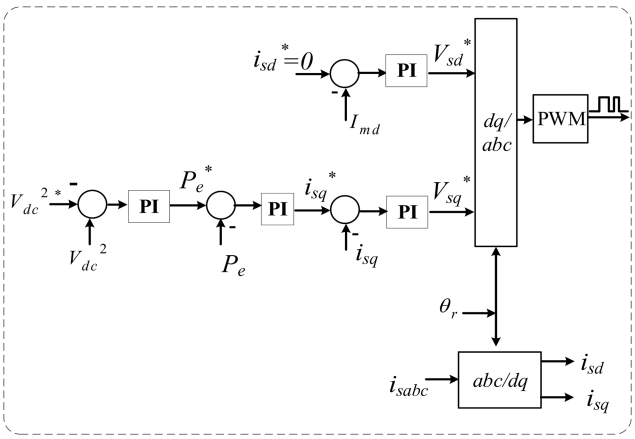

Fig. 3 *Control structure for machine-side converter*

2.2 Machine-side converter control

The machine-side converter (MSC) regulates the electrical power P_e the PMSG extracts from the wind turbine. The PMSG is controlled in the *d-q* frame with the magnetic flux aligned with the rotor angle θ_r. The dynamic equation of the PMSG in the rotor-field coordinates is given by (6) and (7) [14]:

$$V_{sd}=L_d\frac{di_{sd}}{dt}+R_si_{sd}-L_q\omega_ri_{sq} \tag{6}$$

$$V_{sq}=L_q\frac{di_{sq}}{dt}+R_si_{sq}-L_d\omega_ri_{sq}+\lambda_m\omega_r \tag{7}$$

where V_{sq}, V_{sd}, i_{sq}, i_{sd}, L_q, L_d represent the *d-q* component of the stator terminal voltages, current and self-inductances, respectively. λ_m is the rotor flux linkage, R_s is the stator resistance, and ω_r is the rotor speed. The non-salient surface mounted PMSG ($L_q=L_d$) is implemented for this design and the electrical torque T_e and the active power P generated by the PMSG are given by (8) and (9), respectively [14]:

$$T_e=\frac{3}{2}(\lambda_m i_{sq}) \tag{8}$$

$$P_e=\frac{3}{2}(V_{sq}i_{sq}) \tag{9}$$

In this scheme (Fig. 3), the MSC, unlike conventional schemes, controls the DC-link voltage V_{dc}. Based on this design, the PMSG acts as a current source, whose power output P_e is strictly determined by the power reference P_g* from the grid-side converter (GSC). The magnitude of the active power P_e generated by the PMSG is governed by the power balance principle explained in (10), neglecting losses [13]:

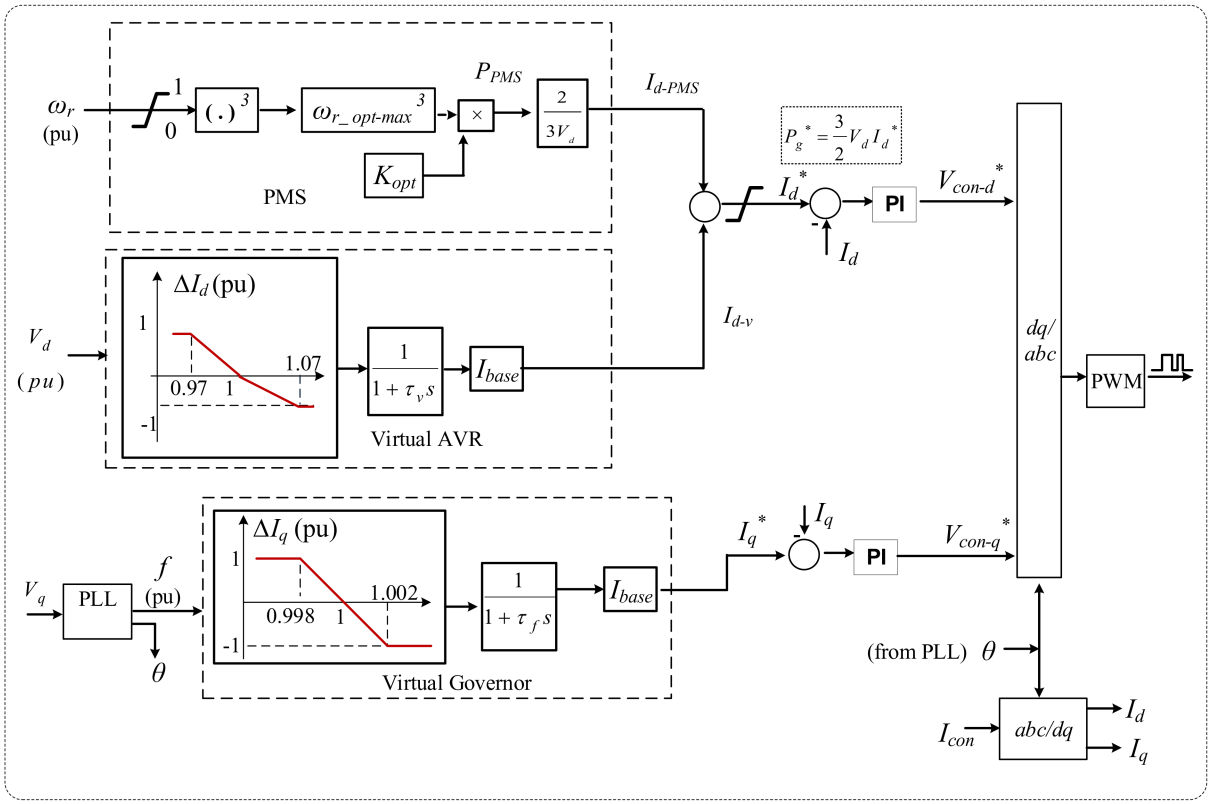

Fig. 4 *Proposed control paradigm for grid-side converter*

$$P_e - P_g = CV_{\mathrm{dc}}\frac{\mathrm{d}V_{\mathrm{dc}}}{\mathrm{d}t} \tag{10}$$

where P_g is the power transferred to the GSC through the DC link and C is the DC-link capacitor. From (10), it is evident that power balance is maintained by regulating V_{dc} at the nominal value. In this scheme, V_{dc} is regulated by comparing ${V_{\mathrm{dc}}}^{2*}$ with ${V_{\mathrm{dc}}}^2$, the PI controller eliminates the steady-state error and provides P_e*, for the power control loop as illustrated in Fig. 3. From (9), it is evident that the active power flow in the system is associated with i_{sq}. Thus, the d-component of the current is usually regulated to zero to minimise ohmic losses and maximise available power [11, 14].

2.3 Grid-side converter control

The GSC is the interface between the WECS and the grid network. It regulates power exchange and ensures safe operation of the WECS and connected loads in all operating modes. The proposed GSC employs a single-control paradigm, which enables MPPT in grid-connected operation, LFPG in islanded mode and LVRT during faults. The base of the GSC employed in this scheme is detailed in [9], the main addition is the proposed power management system (PMS). The GSC consists of three main components: virtual automatic voltage regulator (AVR), virtual governor, and the PMS. The standard d-q frame current controllers have been implemented for this design [14] and the control structure is illustrated in Fig. 4

2.3.1 Virtual governor:: The role of the virtual governor in this scheme is to regulate the frequency f of the microgrid within the nominal value. In grid-connected mode, the PLL ensures the GSC is synchronised with the grid and f is dictated by the grid network. In Islanded operation, the same PLL maintains the q-component of the voltage, V_q at 0 and f is maintained within acceptable standards, by varying f in proportion to the current demand I_q of the reactive load Q_L. Equation (11) explains the I_q–f droop illustrated in Fig. 4 [9]:

$$\Delta I_q = K_f(f - f_0) \tag{11}$$

where the reference frequency $f_0 = 1$ pu and K_f is the droop gain which is chosen according to the acceptable frequency deviations in the adopted standard (50 ± .1 Hz in UK).

The output of the $I_q - f$ droop is passed through a first-order low-pass filter τ_f to add similar damping characteristics available to the governor of the synchronous generator.

where $0.064 < \tau_f < 0.64$ proves suitable for most applications [9].

2.3.2 Virtual AVR: The primary function of the Virtual AVR is to regulate the terminal voltage $V = \sqrt{V_d^2 + V_q^2}$ of the converter. In grid-connected operation, the voltage magnitude is maintained by the grid ($V_d \approx 1$ pu) and the WECS exchanges active power as required or dictated by the transmission system operator (TSO).

However, in islanded mode of operation, V_d is varied in proportion to the current demand I_d of the active load P_L as illustrated in Fig. 4 and described in (12) [9]:

$$\Delta I_d = K_v(V_d - V_0) \tag{12}$$

where V_o is the reference voltage ($V_o = 1$ pu), and K_v is the voltage droop gain.

K_v is determined according to the voltage deviations acceptable by the adopted standards: $0.94 \text{ pu} < V < 1.07$ pu. A 3% safety margin is employed to compensate for losses and voltage drop on transmission line and transformers, hence the droop employed ensures, $0.97 \text{ pu} < V < 1.07$ pu [9]. The output of the $I_d - V$ droop is passed through a first-order low-pass filter to add dynamics which emulate the behaviour of the AVR in the synchronous generator, where $0.02 < \tau_v < 0.1$ proves suitable for most applications [9].

2.3.3 Proposed power management system: The proposed PMS regulates the power demanded from the MSC, enables MPPT in grid-connected operation, and ensures LFPG in islanded mode. The operation of the PMS is corroborated by the virtual AVR. The

Table 1 System parameters

Variable	Value
PMSG rated power	2 MW
rated voltage	0.7 kV
rated rotor speed	3.1 rad/s
DC link voltage	2 kV
DC link capacitance	4.5 mF
transformer rating	415/11 kV
transformers' leakage reactance	8%
transmission line impedance Z_t	$R = 0.16\ \Omega$, $L = 0.6$ mH

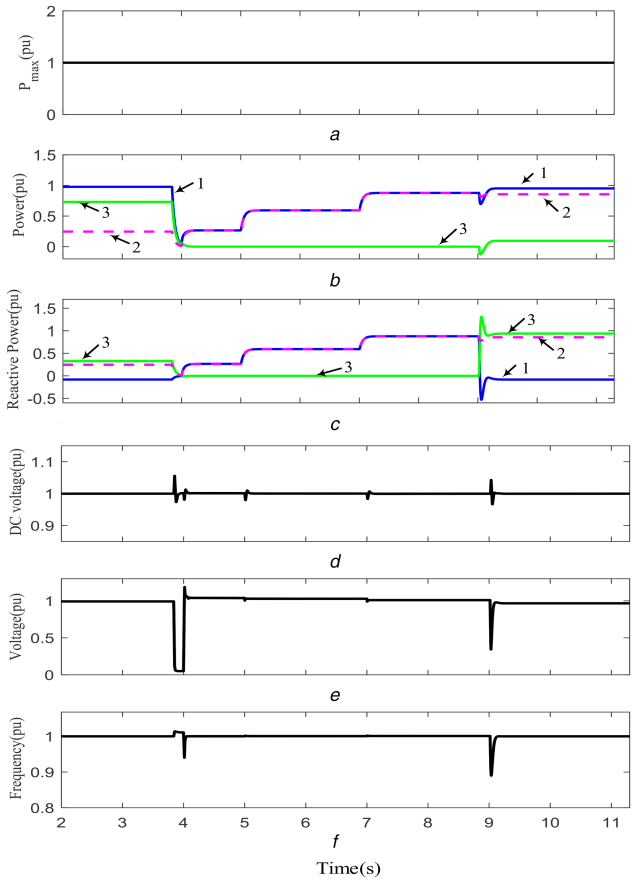

Fig. 5 *Simulation results for WECS in grid connected and islanded mode*
(a) Maximum wind power available, pu P_{max}, ***(b)*** Active power, pu 1 - P_g, 2 - P_L, 3- P_{grid}, ***(c)*** Reactive power, pu 1 - Q_g, 2 - Q_L, 3 - Q_{grid}, ***(d)*** DC-link voltage, pu V_{dc}, ***(e)*** GSC voltage, pu V_d, ***(f)*** Frequency, pu

PMS is integrated to the GSC as illustrated in Fig. 4. In grid-connected operation, the PMS achieves MPPT ($P_{PMS} = P_{max}$) by ensuring $P_{PMS} = K_{opt}\ \omega_r{}^3$, where P_{PMS} is the output power from the PMS, ω_r is the rotor speed and K_{opt} is a constant denoting the optimal ratio required between ω_r and P_m to achieve MPPT.

In grid-connected mode, since the voltage is maintained by the grid, $V_d \approx 1$ pu, the output of the AVR, $I_{d\text{-}v} \approx 0$, hence, $I_{d\text{-PMS}} = I_d{}^*$ (see Fig. 4). In islanded operation (e.g. following a fault on the grid), $P_g{}^*$ is determined by the load demand. Hence, the WECS operates in the SOPPT region to reduce power generation. From Fig. 2, in this region, $\omega_r > \omega_{r\_opt}$ when $P_L < P_{max}$.

As discussed earlier, in islanded operation, the virtual AVR regulates V_d in proportion to the current demand I_d of the load (see (12)). For $P_{PMS} \leq 1$ pu, V_d is regulated within nominal value, $I_d{}^* = I_{d\text{-PMS}} + I_{d\text{-}v}$ (see Fig. 4) and power generated precisely follows the load demand (LFPG).

However, for $\omega_r > \omega_{r\_opt\text{-}max}$, since $P_{PMS} = K_{opt}\ \omega^3$, $P_{PMS} > 1$ pu, which exceeds the AVR capacity. This leads to the increase of V_d beyond the nominal value and eventually the WECS operation becomes unstable. To prevent this scenario, the input ω_r signal is limited to $\omega_{r\_opt\text{-}max} = 1$ pu (see Fig. 4). This ensures that, even though actual rotor speed in SOPPT may be greater than 1 pu, the maximum input signal to the PMS is $\omega_{r\_opt\text{-}max} = 1$ pu.

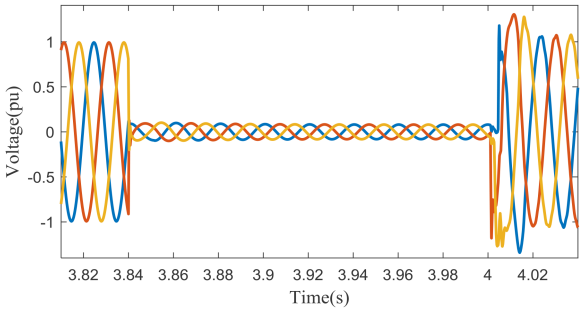

Fig. 6 *Three-phase voltage waveform of V during fault*

Based on this design, the PMS seamlessly enables MPPT when grid-connected and LFPG in islanded mode without switching control paradigms. It is noted that the WECS blades are not designed to be pitched constantly, as it may reduce the lifetime and increase the required maintenance. Moreover, the slow dynamics of the pitch controller makes it unsuitable for responding to the continuously varying load conditions in the microgrid [7]. Therefore, the pitch controller is only activated for $\omega_r > \omega_{r\text{-rated}}$ or $P_m > P_{max}$.

3 Simulation results

The model in Fig. 1 was simulated in the MATLAB/SIMULINK environment. The load PF was maintained at 0.9 lagging all through the simulation. Two scenarios have been simulated and discussed. The system parameters for the WECS are given in Table 1 below:

3.1 Grid-connected to islanded operation

3.1.1 Grid operation (2–4 s): The WECS is connected to the grid and V and f are maintained by the grid. From Fig. 5, it is observed that the WECS is operating at MPPT $P_g = P_{max}$ and the excess power not consumed by the load P_L is transferred to the grid. It is also observed that Q_L is supplied by the grid Q_{grid}. The slight difference observed between Q_{grid} and Q_L is a result of the transformer's leakage reactance. At 3.84 s, a three-phase fault occurs at the grid side, $V \approx 0$. It is observed that the WECS seamlessly rides through the fault as V_{dc} and f are within the nominal value.

The fault is not cleared within 0.16 s, and as stipulated in [15] the WECS is disconnected from the grid by opening the circuit breaker (CB).

3.1.2 Islanded operation (4–9 s): In this operation mode, the WECS reduces generation and operates in the SOPPT region to ensure LFPG. As illustrated in Fig. 5, P_g and Q_g precisely follow the load demand P_L and Q_L, respectively. Fig. 5 also shows that the AVR and virtual governor regulated V and f within nominal values during this period. The three-phase voltage waveform of V in Fig. 6 illustrates that the voltage and frequency are well-controlled, with minimal overshoot and waveform distortion during and after fault occurrence.

3.1.3 Grid reconnection (9–12 s): At $t = 9$ s, the CB is closed and the WECS connected to the grid. As illustrated in Fig. 5, the transition to grid is seamless, V and f are within nominal values. Immediately after the grid is restored, the WECS resumes generation at MPPT.

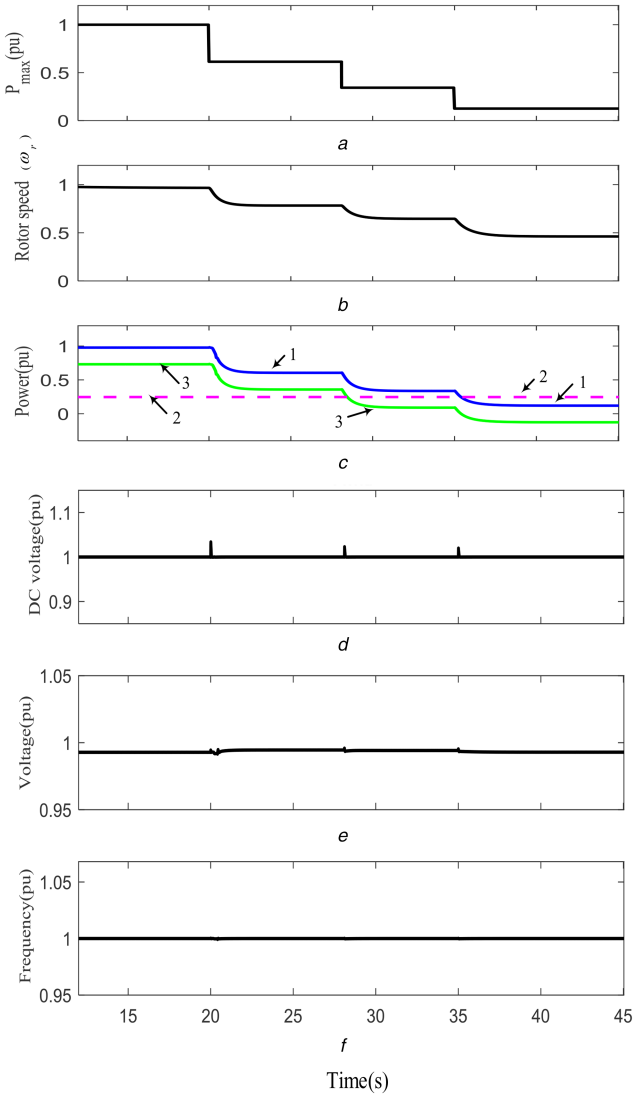

Fig. 7 *Simulation results for WECS under varying wind conditions*
(a) Maximum power wind power available, pu $P_{\max}$, ***(b)*** Rotor speed, pu ω_r, ***(c)*** Active power, pu 1 – P_g, 2 – P_L, 3 – P_{grid}, ***(d)*** DC-Link voltage, pu V_{dc}, ***(e)*** GSC voltage, pu V_d, ***(f)*** Frequency, pu

3.2 Grid operation under varying wind conditions

For this test, the available wind power $P_{\max}$ is varied in steps, while P_L is maintained at 0.25 pu. From Fig. 7, it is observed that as $P_{\max}$ reduces, ω_r decreases proportionally to maintain optimal ratio with $P_{\max}$ as required for MPPT operation. At $t = 35$ s, $P_{\max} < P_L$ and the P_{grid} supplies the deficit power to the load. It is observed that throughout the operation the system parameters V_{dc}, V, and f are within nominal values.

The above results demonstrate that the proposed PMS effectively manages power flow, achieves seamless operation, and enables MPPT and LFPG operation in grid and island mode, respectively, without switching control paradigms.

4 Conclusion

This paper introduces a new control paradigm for the seamless operation of PMSG-based WECS in both grid-connected and islanded operation. It employs a single-control paradigm, which achieves MPPT in grid-connected operation, LFPG in islanded operation and LVRT during faults. The operation of the proposed control structure has been validated in MATLAB/SIMULINK and the results confirm that the proposed PMS seamlessly enables MPPT and LFPG operation in grid and island modes, respectively, without switching control paradigms.

5 References

[1] Liu, J., Miura, Y., Ise, T.: 'Comparison of dynamic characteristics between virtual synchronous generator and droop control in inverter-based distributed generators', *IEEE Trans. Power Electron.*, 2016, **31**, (5), pp. 3600–3611

[2] Monica, P., Kowsalya, M.: 'Control strategies of parallel operated inverters in renewable energy application: A review', *Renew. Sust. Energy Rev.*, 2016, **65**, pp. 885–901

[3] Karimi-Ghartemani, M.: 'Universal integrated synchronization and control for single-phase DC/AC converters', *IEEE Trans. Power Electron.*, 2015, **30**, (3), pp. 1544–1557

[4] Egwebe, A.M., Fazeli, M., Igic, P., *et al.*: 'Implementation and stability study of dynamic droop in islanded microgrids', *IEEE Trans. Energy Convers.*, 2016, **31**, (3), pp. 821–832

[5] Jouini, T., Arghir, C., Dorfler, F.: 'Grid-forming control for power converters based on matching of synchronous machines', arXiv preprint arXiv:1706.09495, 2017

[6] Erlich, I., Korai, A., Neumann, T., *et al.*: 'New control of wind turbines ensuring stable and secure operation following islanding of wind farms', *IEEE Trans. Energy Convers.*, 2017, **32**, (3), pp. 1263–1271

[7] Yuan, X., Li, Y.: 'Control of variable pitch and variable speed direct-drive wind turbines in weak grid systems with active power balance', *IET Renew. Power Gener.*, 2014, **8**, (2), pp. 119–131

[8] Rizo, M., Liserre, M., Bueno, E., *et al.*: 'Universal wind turbine working in grid-connected and island operating modes', *Math. Comput. Simul.*, 2013, **91**, pp. 41–51

[9] Fazeli, M., Holland, P.: 'Universal and seamless control of distributed resources-energy storage for ll operational scenarios of microgrids', *IEEE Trans. Energy Convers.*, 2017, **32**, (3), pp. 963–973

[10] Tan, Y., Muttaqi, K.M.: 'Enhanced frequency response strategy for PMSG based wind energy conversion system using ultracapacitor in remote area power supply systems'. 2015 IEEE Industry Applications Society Annual Meeting, Addison, TX, USA, 2015, pp. 1–8

[11] Jae Ik, Y., Jaewoo, K., Park, J.W.: 'Converter control of PMSG wind turbine system for inertia-free stand-alone microgrid'. 2016 IEEE Industry Applications Society Annual Meeting, Portland, OR, USA, 2016, pp. 1–8

[12] Errami, Y., Ouassaid, M., Maaroufi, M.: 'Control of a PMSG based wind energy generation system for power maximization and grid fault conditions', *Energy Procedia*, 2013, **42**, pp. 220–229

[13] Kim, J., Lee, S.H., Park, J.W.: 'Inertia-free stand-alone microgrid, part II: inertia control and stability with PMSG wind turbine system'. 2017 IEEE Industry Applications Society Annual Meeting, Cincinnati, OH, USA, 2017, pp. 1–8

[14] Yazdani, A., Iravani, R.: '*Voltage-Sourced converters in power systems: modeling, control, and applications*' (Wiley, Hoboken, NJ, USA, 2010)

[15] Duong, M.Q., Nguyen, H.H., Le, K.H., *et al.*: 'Simulation and performance analysis of a new LVRT and damping control scheme for DFIG wind turbines'. 2016 IEEE Int. Conf. on Sustainable Energy Technologies (ICSET), Hanoi, Vietnam, 2016, pp. 288–293